AIP Journal of Applied Physics

# Structural, electrical, and optical properties of atomic layer deposition Al-doped ZnO films

Parag Banerjee, Won-Jae Lee, Ki-Ryeol Bae, Sang Bok Lee, and Gary W. Rubloff

Citation: J. Appl. Phys. 108, 043504 (2010); doi: 10.1063/1.3466987
View online: http://dx.doi.org/10.1063/1.3466987
View Table of Contents: http://jap.aip.org/resource/1/JAPIAU/v108/i4
Published by the American Institute of Physics.

## Additional information on J. Appl. Phys.

Journal Homepage: http://jap.aip.org/
Journal Information: http://jap.aip.org/about/about_the_journal
Top downloads: http://jap.aip.org/features/most_downloaded
Information for Authors: http://jap.aip.org/authors

ADVERTISEMENT

Downloaded 17 Apr 2013 to 143.248.118.125. This article is copyrighted as indicated in the abstract. Reuse of AIP content is subject to the terms at: http://jap.aip.org/about/rights_and_permissions

# Structural, electrical, and optical properties of atomic layer deposition Al-doped ZnO films

Parag Banerjee,[1,2] Won-Jae Lee,[1,3,a)] Ki-Ryeol Bae,[3] Sang Bok Lee,[4,5] and Gary W. Rubloff[1,2,6,b)]
[1]Department of Materials Science and Engineering, University of Maryland, College Park, Maryland 20742, USA
[2]Institute for Systems Research, University of Maryland, College Park, Maryland 20742, USA
[3]Department of Nano Engineering, Dongeui University, Busan 614-714, Republic of Korea
[4]Department of Chemistry and Biochemistry, University of Maryland, College Park Maryland 20742, USA
[5]Graduate School of Nanoscience and Technology (WCU), Korea Advanced Institute of Science and Technology, 335 Gwahangno, Yuseong-gu, Daejeon 305-701, Republic of Korea
[6]Institute for Research in Electronics and Applied Physics, University of Maryland, College Park, Maryland 20742, USA

(Received 12 February 2010; accepted 26 June 2010; published online 17 August 2010)

Al-doped ZnO (AZO) films of $\sim 100$ nm thickness with various Al doping were prepared at 150 °C by atomic layer deposition on quartz substrates. At low Al doping, the films were strongly textured along the [100] direction, while at higher Al doping the films remained amorphous. Atomic force microscopy results showed that Al–O cycles when inserted in a ZnO film, corresponding to a few atomic percent Al, could remarkably reduce the surface roughness of the films. Hall measurements revealed a maximum mobility of 17.7 $cm^2/V\ s$. Film resistivity reached a minima of $4.4 \times 10^{-3}\ \Omega$ cm whereas the carrier concentration reached a maxima of $1.7 \times 10^{20}\ cm^{-3}$, at 3 at. % Al. The band gap of AZO films varied from 3.23 eV for undoped ZnO films to 3.73 eV for AZO films with 24.6 at. % Al. Optical transmittance over 80% was obtained in the visible region. The detrimental impact of increased Al resulting in decreased conductivity due to doping past 3.0 at. % is evident in the x-ray diffraction data, as an abrupt increase in the optical band gap and as a deviation from the Burstein–Moss effect. © *2010 American Institute of Physics*. [doi:10.1063/1.3466987]

## I. INTRODUCTION

Since zinc oxide (ZnO) is a semiconductor material with a wide band gap of 3.27 eV and a large exciton binding energy of 60 meV at room temperature, ZnO-based thin films have been used for several applications such as transparent conducting oxide (TCO), ultraviolet light emitters, solar cell windows, and bulk acoustic wave devices.[1–4] Among various materials for TCO applications, Al-doped ZnO (AZO) film is a particularly attractive material because of its excellent properties, such as higher thermal stability, good resistance against damage by hydrogen plasma and low cost of fabrication, compared to indium tin oxide.[5] Therefore, a number of fabrication techniques such as sputtering,[2,3] pulsed laser deposition (PLD),[4] and chemical vapor deposition (CVD) (Ref. 6) have been adopted to deposit AZO thin films.

On the other hand, the reduction of thin films to nanometer dimensions for new technologies requires precise control of film thickness, conformality, and morphology. A lower deposition temperature is also required for deposition onto plastic substrates for flexible electronics and to minimize interlayer diffusion in nanoscale devices. These requirements can be achieved by an atomic layer deposition (ALD) technique which can realize film growth controlled to within a single atomic layer by means of a binary reaction sequence chemistry.[7]

Past work on ALD-based AZO films has involved studying the structural, morphological and electrical properties of AZO films across the entire composition spectrum.[8–10] However, optical characterization which may yield band gap information of these films have not been evaluated. Hall measurements which provide complete information on conduction characteristics including resistivity, mobility, and carrier concentration is also lacking. Both these measurements are important as they provide a physical and atomistic view of the effect of Al doping in ZnO grown via ALD. Therefore, in this study AZO films were deposited at a low temperature of 150 °C by the ALD method and then systematically analyzed for its structural, electrical and optical properties which included optical characterization and Hall measurements. We fabricated AZO thin films with various Al doping concentrations by inserting an $Al_2O_3$ ALD cycle after every "n" ZnO cycles, varying n from 40 to 5, to achieve different $ZnO/Al_2O_3$ ratios. Since there are only a few reports on low temperature, ALD ZnO-based films prepared by the ALD technique,[8–12] this work adds valuable information on the structure-property relationship in ALD-based AZO films.

## II. EXPERIMENTAL

AZO thin films were deposited at 150 °C using a BENEQ TFS-500 ALD viscous-flow reactor. High purity quartz glasses were used as the substrate for AZO film growth. Diethyl zinc [DEZ, $Zn(C_2H_5)_2$] and distilled (DI)

a)Electronic mail: leewj@deu.ac.kr.
b)Electronic mail: rubloff@umd.edu.

 © 2010 American Institute of Physics

Downloaded 17 Apr 2013 to 143.248.118.125. This article is copyrighted as indicated in the abstract. Reuse of AIP content is subject to the terms at: http://jap.aip.org/about/rights_and_permissions

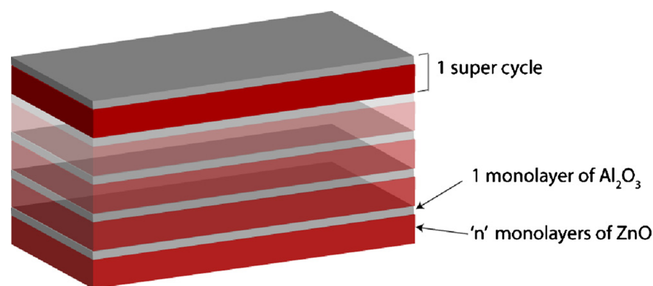


FIG. 1. (Color online) Schematic diagram of the film stack used to make various AZO films by ALD.

water were used as precursors to deposit ZnO films at a growth per cycle ($GPC_{ZnO}$) of 0.2 nm/cycle. Pulse times for DEZ and DI water cycles were kept at 250 ms. High purity nitrogen was adopted as a purging gas. For preparing ALD-$Al_2O_3$ films at 150 °C, trimethyl aluminum [TMA, $Al(CH_3)_3$] and DI water were used as precursors at a $GPC_{Al_2O_3}$ of 0.1 nm/cycle. Pulse times for TMA and DI water cycles were kept at 250 ms. The GPC for ZnO and $Al_2O_3$ was established during deposition of pure, individual ZnO and $Al_2O_3$ ALD films, respectively, in each case the process recipe achieving the characteristics (uniformity, precursor dose saturation, etc.) expected for ALD.

To achieve a particular at. % Al doping into ZnO films, a single TMA-DI water cycle was inserted after a set number of DEZ-DI water cycles. This constituted one "supercycle" of AZO, composed of n cycles of DEZ-DI water followed by one cycle of TMA-DI water. Figure 1 shows the schematic diagram of the film stack used to make various AZO films by the ALD method. Here n was varied from 40 to 5 to produce various compositions of AZO films. The supercycles were calculated to target a resultant thickness of ~100 nm for each AZO film (Table I). Thickness of the films were measured using spectroscopic ellipsometry (Sopra GES5E) and optical models discussed elsewhere.[13] An x-ray diffractometer (X'pert MPD, Panalytical, 40 kV, 30 mA) was used to investigate structural properties of the thin films. Energy-dispersive x-ray spectroscopy (EDX) was done on a Hitachi SU70 scanning electron microscope (SEM) using a Bruker silicon drift detector attached to the SEM column with a beam energy of 20 keV. The surface morphologies of the thin films were investigated by a scanning probe microscope (SPM) in the atomic force microscope (AFM) mode (SPA-400, Seiko Instruments). The electrical properties of the thin films were measured by van der Pauw method at room temperature using a Hall Effect measurement system (Ecopia HMS 3000). A spectrophotometer (Shimadzu RF-1501) was used to measure the transmittances of the thin films in the wavelength range of 250–900 nm.

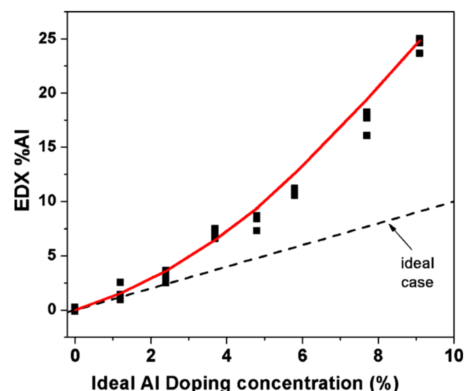


FIG. 2. (Color online) Variation in true at. % Al in AZO films measured via EDX with the ideal at. % Al calculated as ideal at %Al $=(GPC_{Al_2O_3}/GPC_{Al_2O_3}+nGPC_{ZnO})$ due to the processing sequence adopted for doping the AZO films. The dashed line shows, in the ideal case, that true at. % Al should be equal to the ideal at. % Al. The fit (solid) is a phenomenological fit to the data and is described in text.

## III. RESULTS AND DISCUSSION

The thickness of the films were found to be off-target for the higher at. % Al samples. Similarly, the ideal at. % Al given by ideal at. $\%Al=(GPC_{Al_2O_3}/GPC_{Al_2O_3}+nGPC_{ZnO})$ was found to deviate at higher at. % Al samples as well. This is verified using EDX and is presented in Fig. 2. For instance, in case of the AZO film grown with n=10, the target thickness was calculated to be 100.8 nm and the "ideal" at. % Al was 4.8%. However, the true thickness was found to be 96.8 nm and a true at. % Al of 8.1% was obtained for this sample using EDX. It is known that ZnO encounters barrier to growth on $Al_2O_3$ and thus both thickness and at. % Al are affected in these samples.[9] Henceforth, at. % Al will be given in terms of true at. % Al as determined by EDX. No post-deposition, thermal annealing was performed.

TABLE I. List of samples used for obtaining data showing the ratio of Zn to Al cycles used to obtain various Al doping concentration. Here, n is the number of DEZ-DI water cycles inserted between consecutive TMA-DI water cycles. This constitutes a single supercycle. By repeating the supercycles, estimated total thickness is obtained. The true total thickness is based on measurement using spectroscopic ellipsometry. The estimated at. % Al is calculated by the method shown in text. The true at. % Al doping is obtained via EDX.

| Sample | n | Thickness of one supercycle (nm) | Total number of supercycles | Estimated total thickness (nm) | True total thickness (nm) | Estimated Al (at. %) | True at. % Al (via EDX) |
|---|---|---|---|---|---|---|---|
| ZnO | N/A | N/A | N/A | 100.0 | 103.0 | 0 | 0 |
| Zn:Al=40:1 | 40 | 8.1 | 12 | 97.2 | 101.0 | 1.2 | 1.5 |
| Zn:Al=20:1 | 20 | 4.1 | 24 | 98.4 | 97.3 | 2.4 | 3.0 |
| Zn:Al=13:1 | 13 | 2.7 | 37 | 99.9 | 95.0 | 3.7 | 7.3 |
| Zn:Al=10:1 | 10 | 2.1 | 48 | 100.8 | 96.8 | 4.8 | 8.1 |
| Zn:Al=8:1 | 8 | 1.7 | 59 | 100.3 | 96.8 | 5.9 | 10.9 |
| Zn:Al=6:1 | 6 | 1.3 | 77 | 100.1 | 89.1 | 7.7 | 17.3 |
| Zn:Al=5:1 | 5 | 1.1 | 91 | 100.1 | 86.3 | 9.1 | 24.6 |

Downloaded 17 Apr 2013 to 143.248.118.125. This article is copyrighted as indicated in the abstract. Reuse of AIP content is subject to the terms at: http://jap.aip.org/about/rights_and_permissions

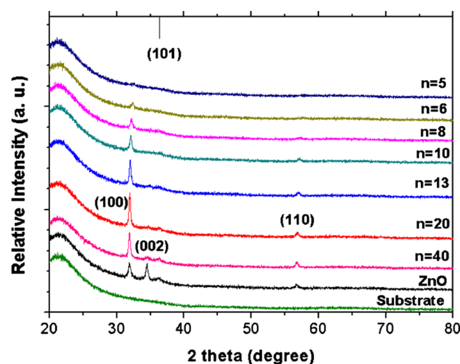


FIG. 3. (Color online) XRD patterns for AZO films prepared by different cycle combination, where n is the number of DEZ-DI water cycles separated by two TMA-DI water cycles. Lower the n, higher the at. % Al doping.

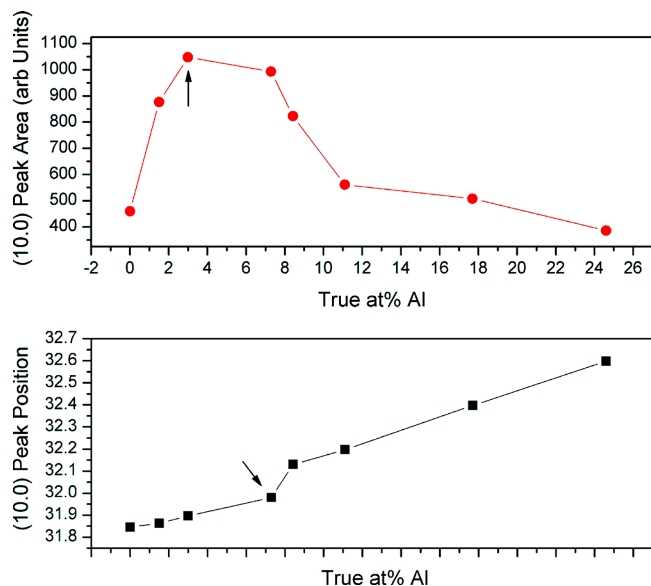


FIG. 4. (Color online) (a) Area under the (100) peak for AZO films with different Al concentration. The peak areas have been normalized with respect to at. % Zn and thickness of the films. The area maximizes at 3.0 at. % Al (shown by the arrow). (b) Peak position of the (100) as a function of at. % Al. There is a kink in the linear trend observed at 7.3 at. % Al.

To phenomenologically model the suppressed growth of ZnO on $Al_2O_3$, it was assumed that the areal density of Zn atoms as a result of reduced adsorption of DEZ on $Al_2O_3$ follows an exponential behavior given by $\rho_{Zn}=\rho_{Zn}^0\{1-\exp[-(n/\tau)]\}$ where $\rho_{Zn}^0$ is the ideal, areal atomic density of Zn in ZnO, n is the nth cycle number after $Al_2O_3$ deposition, and $\tau$ is the cycle number required for $\rho_{Zn}$ to reach 63.2% of $\rho_{Zn}^0$-the ideal areal density. This assumption is valid since it is expected that after a thick enough layer of ZnO is deposited on $Al_2O_3$ the GPC for ZnO will be close to that observed in pure ALD ZnO films. Thus, this analysis quantifies the kinetics of the recovery behavior of ZnO deposition. Since only one cycle of $Al_2O_3$ is used for alloying, we assume that the areal atomic density of Al in $Al_2O_3$ is constant across all the samples and, for simplicity, is equal to the equilibrium value found in pure $Al_2O_3$. Using the planar atomic density of Zn in ZnO given by $\rho_{Zn}^0=8.34\times10^{14}/cm^2$ and Al in $Al_2O_3$ as $\rho_{Al}^0=4.44\times10^{14}/cm^2$,[8] the at. % Al can be modeled by simply integrating the atomic density dependence on cycle number, as given above, to obtain $at\%Al=100/[(\rho_{Zn}/\rho_{Al})\{n-\tau+\tau\exp[-(n/\tau)]\}+1]$ and comparing it with the EDX data. From this equation, the value of $\tau$ is found to be $\sim$6 and is shown in solid in Fig. 2. Thus, it takes approximately 6 cycles of ZnO to recover 63.2% of its original atomic areal density when depositing on a single monolayer of $Al_2O_3$. The recovery behavior given by $\tau\sim6$ is expected to change if more than one monolayer of $Al_2O_3$ is used in alloying.

Next, the structural properties of the films were analyzed. Figure 3 shows x-ray diffraction (XRD) patterns for AZO films prepared varying n, the number of DEZ-DI water cycles inserted for every TMA-DI water cycle. The crystalline state and crystal orientation of the as-deposited films were found to change with n. ZnO films grown without any TMA-DI water cycle exhibited a polycrystalline state having (100), (002), (101), and (110) orientation. However as $Al_2O_3$ is introduced, the (002) peak disappears and the intensity of the (100) peak becomes dominant reaching a maximum at n=20. With further decrease in n i.e., increased Al doping, the (100) peak diminishes in intensity and at n=5 no peak is observed, which indicates that the AZO film at 24.6 at. % Al is amorphous.

The area under the (100) peak is plotted in Fig. 4(a). Because the films have various thicknesses, care has to be taken to interpret the results since crystallization behavior is often thickness dependent. In our case, the area of the (100) peak is normalized to the amount of Zn present in the individual films. This is done by using the ratio of Zn:Si peaks from the EDX data obtained earlier for films deposited on quartz substrates (see Ref. 14). For a constant composition, thinner films will have a lower Zn:Si ratio than thicker films. Similarly, for a constant thickness higher at. % Zn films will have a higher Zn:Si ratio. Thus, the EDX Zn:Si ratio provides a convenient method to normalize data where thickness and composition are convoluted with one another. As stated before, the area of the (100) peak goes through a maxima at 3 at. % Al (n=20) and then decreases subsequently. It is well known that the [002] direction i.e., the c-axis, is the preferential orientation commonly observed in ZnO and doped ZnO films prepared by various deposition techniques such as sputtering, PLD, and CVD.[13,15,16] However, ALD processes have been shown to yield a texturing effect which is dependent on temperature, pulsing and purging times.[11,17,18] The [100] orientation i.e., the a-axis, is found to occur in a narrow temperature window that spans from 155–220 °C and has been attributed to the breakdown of negatively charged hydrocarbon ligands in DEZ which disturb the charge distribution on (002) planes.[17]

In the current scheme however, it was found that [100] direction is dominant when $Al^{3+}$ is introduced as a dopant. To explain this behavior, it is worthwhile to note that the (002) plane consists of alternate planes of $Zn^{2+}$ and $O^{2-}$ and thus is charged positively or negatively, respectively, depending on surface termination. On the other hand, the (100) plane is a charge neutral surface consisting of alternate rows of $Zn^{2+}$ and $O^{2-}$ ions on the surface. Thus, it is conceivable that the layer-by-layer growth during ALD may cause the $Al^{3+}$ ions to disturb the charge neutrality of the (100) plane thereby affecting its surface energy and causing its preferen-

Downloaded 17 Apr 2013 to 143.248.118.125. This article is copyrighted as indicated in the abstract. Reuse of AIP content is subject to the terms at: http://jap.aip.org/about/rights_and_permissions

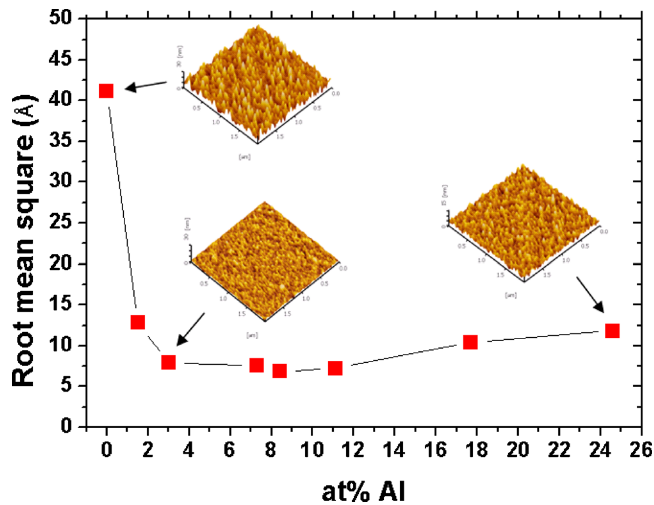


FIG. 5. (Color online) The rms roughness and associated surface morphologies obtained via AFM for AZO films as a function of at. % Al.

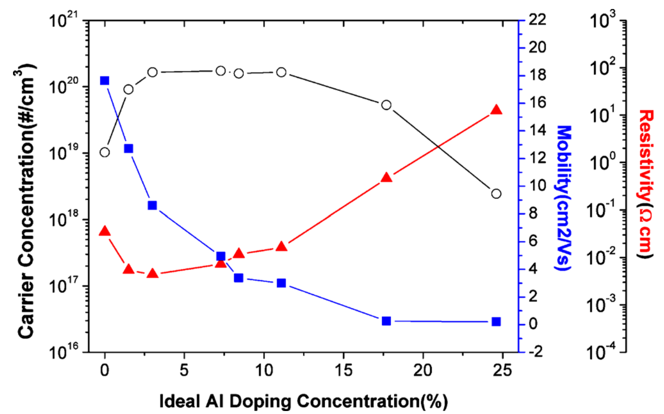


FIG. 6. (Color online) Room temperature carrier concentration (-○-left axis), mobility (-■-right axis), and resistivity (-▲-right axis, offset) as a function of at. % Al doping for AZO films.

tial growth. Indeed, it has been reported[10] that an exchange reaction between TMA and the ZnO surface is possible. This may lead to texturing effects in the films not found in other modes of deposition or growth.

The (100) peak position is plotted in Fig. 4(b). The peak position increased with increasing Al concentration in AZO films—linearly with doping with a "kink" at ~7.3 at. % Al. This implies that Al addition into ZnO film reduces the d-spacing along the [100] direction. We attribute this to $Al^{3+}$ ions substitutionally doping the $Zn^{2+}$ at random sites. The $Zn^{2+}$ ionic radius is 72 pm compared to the $Al^{3+}$ of 54 pm and could thus result in smaller interplanar distances.[19] Recently, Yoshioka *et al.*,[20] have studied the ZnO-$Al_2O_3$ system and concluded that a stretching along c-axis occurs past 8 at. % Al as well. This has been attributed to the presence of a metastable, homologous phase where the $Al^{3+}$ ion has a coordination number (CN) of 5 even though it resides on a $Zn^{2+}$ site (CN=6). Since their films were c-axis oriented no information on the *d*-spacing along the a-axis were provided but it is conceivable that the stretching along the c-axis along with a smaller $Al^{3+}$ ionic radius can cause a decrease in the *d*-spacing along the [100] direction. The issue of metastable phase formation will be touched upon again while discussing the correlation between structural, electrical and optical properties. The presence of a spinel $ZnAl_2O_4$ phase can be ruled out since it occurs at a lower $2\theta$ than the (100) peak in the XRD profile.[21] The absence of the spinel phase in ALD AZO films have been reported by Elam *et al.*[9] as well.

The surface morphologies of the thin films with a scanning area of $2\times 2$ $\mu m^2$ were analyzed by using a SPM in the AFM mode. Figure 5 shows the root mean square (rms) surface roughness for AZO thin films as a function of at. % Al. AFM images of three representative films—pure ZnO, n=20 (3 at. % Al) and 5 (24.6 at. % Al) is also shown in the inset of the figure. It is found that the surface roughness is strongly dependent on at. % Al. The roughness of ZnO films grown without the TMA-DI water cycle was 4.1 nm and then dramatically decreased with increasing Al doping. As the at. % Al reached over 3.0%, the rms roughness values of AZO films saturated to around 0.8 nm and then slightly increased to 1.0–1.1 nm for over 17.3 at. % Al. This AFM result shows that even a single cycle of TMA-DI water separated by 40 cycles of DEZ-DI water can remarkably reduce the roughness of AZO films. Similar results have been reported by Elam *et al.*,[10] for nanolaminate $Al_2O_3$-ZnO films and is attributed to the $Al^{3+}$ ions substituting surface $Zn^{2+}$ ions thus stymieing ZnO crystal growth. The slight increase in the roughness at higher at. % Al has been attributed to TMA etching of the ZnO surface, although we find no evidence of the sudden increase in rms roughness at similar at. % Al as reported by Elam and George.[8] Perhaps the discrepancy lies in the difference in analysis techniques used to determine at. % Al in the films. Whereas the present study uses EDX, Elam *et al.*, have used inductively coupled plasma atomic emission spectroscopy to determine Al doping in the films. Notwithstanding this, the roughness results highlight AZO's potential use as a TCO, especially where low temperature and precise control over film uniformity, smoothness, conformality and thickness is required.

Hall measurements were carried out at room temperature to investigate the electrical properties of AZO thin films. This is shown as a function of at. % Al in Fig. 6. Note that all the films, both AZO and pure ZnO, were n-type semiconductors. In the case of pure ZnO film, the carrier concentration and the mobility were $1.0\times 10^{19}$ $cm^{-3}$ and 17.7 $cm^2/V$ s, respectively. As the Al doping increased, the carrier concentration of AZO films at first increased rapidly and then saturated to $\sim 1.7\times 10^{20}$ $cm^{-3}$. For Al doping over 11 at. %, the carrier concentration of AZO films was abruptly reduced. The mobility of AZO films continuously decreased from 17.7 to 0.2 $cm^2/V$ s while Al doping increased from 1.5 to 24.6 at. %. Furthermore, the lowest resistivity of $4.4\times 10^{-3}$ Ω cm was obtained for AZO films grown with 3.0 at. % Al (n=20). This resistivity value is higher than those reported for AZO films from other deposition processes. However, note that the films are only ~100 nm thick, whereas past work has focused on films with higher thicknesses. Furthermore, the lowest resistivity is obtained at an AZO composition of 3 at. % Al which is in line with prior reports, e.g., Hüpkes *et al.*,[22] report a minimum resistivity ($2.4\times 10^{-4}$ Ω cm) for 700–900 nm AZO films at 3 at. % Al. Further increase in at. % Al increased the resistivity. Interest-

Downloaded 17 Apr 2013 to 143.248.118.125. This article is copyrighted as indicated in the abstract. Reuse of AIP content is subject to the terms at: http://jap.aip.org/about/rights_and_permissions

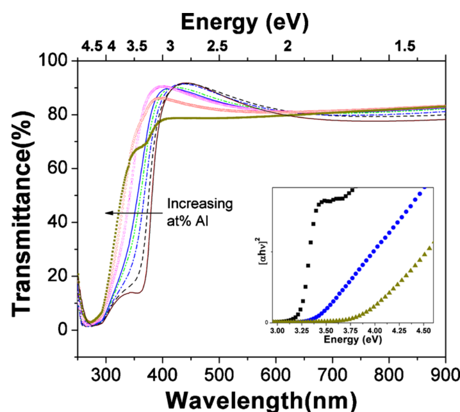


FIG. 7. (Color online) Transmittance as a function wavelength (bottom x-axis) and energy (top x-axis) for various Al concentrations in AZO films. The absorption edge blueshifts for higher at. % Al doping. Inset shows Tauc plots for three representative samples—■ for 0 at. % Al, ● for 7.30 at. % Al, and ▲ for 24.6 at. % Al.

ingly, the 3.0 at. % Al sample also showed the highest XRD (100) area under the peak and the lowest surface roughness, indicating that both the degree of crystallinity and surface roughness play an important role in determining the resistivity of AZO films. These results are consistent with Matthiessen's rule for electrical conductivity which takes into account contributions to resistivity from thermal vibrations (i.e., phonons), impurities and defects.[23] Thus, highly crystalline films with smoother surface morphology would lead to less carrier scattering, higher mobilities and therefore, improved conductivity. Similar results linking conductivity to grain morphology are reported by Lu *et al.*,[24] who report a maxima in the grain size and a minima in resistivity at 4.0 at. % Al for sputtered AZO films.

For TCO application, the transmittances (T) of AZO thin films were measured at room temperature by a double-beam spectrophotometer. The transmittance spectra for various samples are shown in Fig. 7 in the wavelength range of 250–900 nm. All of the thin films prepared with various Al doping levels showed as high as 80%–92% optical transmission in the visible range, which is important for TCO applications such as solar cell windows. The band gap of AZO thin films can be measured by fitting the sharp absorption edges. In order to calculate the band gap energies of the thin films, Tauc plots were drawn where it was assumed that the absorption coefficient $\alpha \sim -\ln(\mathrm{T})$ corresponding to the direct band gap of the wurtzite structure of ZnO. A plot of $[\alpha \times (h\upsilon)]^2$ against the photon energy ($h\upsilon$) was drawn and the sharp absorption edge could be accurately determined for the thin film by the linear fit (Fig. 7 inset). The absorption edge undergoes a blueshift with increasing Al doping.

To understand the increase in the energy of the absorption edge with Al doping further, the optical band gap energies are plotted with at. % Al in Fig. 8(a). It was observed that the optical band gap of AZO thin films changed from 3.23 to 3.73 eV for Al doping varying from 0 at. % to 24.6 at. %, respectively. The ideal band gap of pure ZnO is 3.27 eV and that of $Al_2O_3$ is 8.7 eV.[1,25] Thus, the increase in band gap is to be expected with increase in at. % Al. However, the band gap of AZO increases abruptly at ~7.3 at. % Al. This corresponds to the kink observed in the XRD peak position [Fig. 4(b)], providing further indication that at low at. % Al, $Al^{3+}$ ions substitutionally occupy the $Zn^{2+}$ sites and perturb the properties of pure ZnO. However at higher at. % Al, three scenarios are possible (a) phase segregation of Al from ZnO, (b) formation of a spinel $ZnAl_2O_4$ (Ref. 21 or, (c) formation of a metastable $(ZnO)_3(Al_2O_3)$ phase.[20] Al phase segregation in a ZnO matrix would result in increased conductivity of the resulting film. Since electrical data does not support this fact and no sign of a spinel-like phase in XRD is detected, the discontinuities observed in XRD and optical data and the loss in carrier concentration most likely stem from the presence of the metastable phase as predicted by Yoshioka *et al.*[20] The low temperature of deposition and ALD's monolayer-by-monolayer growth mechanism may result in formation of thermodynamically metastable phases. It should also be noted that the thickness of the AZO films (~100 nm) in this work is one of the thinnest studied and the resultant stress and high interface/surface to volume ratio in these films may play a role in energetically favoring the nucleation and growth of such a phase as well.

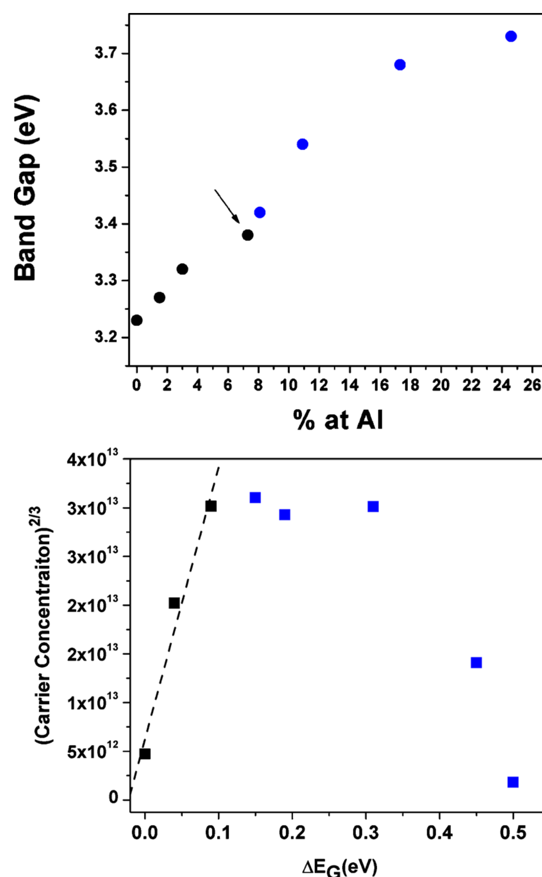


FIG. 8. (Color online) (a) Band gap as a function of Al concentration for AZO films prepared with different Al doping concentration. (b) The relationship between (carrier concentration)$^{2/3}$ and the band gap change, $\Delta E_G$. The linear trend is due to the Burstein–Moss effect which occurs till ~3.0 at. % Al.

Finally, the increase in band gap observed in TCO's is normally believed to be due to the Burstein–Moss effect.[26,27] This effect has been well characterized for AZO films[24,28–30] and can be explained as follows—since ZnO thin film is naturally n-type, addition of donor $Al^{3+}$ ions raises the Fermi

Downloaded 17 Apr 2013 to 143.248.118.125. This article is copyrighted as indicated in the abstract. Reuse of AIP content is subject to the terms at: http://jap.aip.org/about/rights_and_permissions

level of AZO films into the conduction band making the films completely degenerate and hence the absorption edge shifts to energies higher than the actual band gap of the material. Ignoring many-body effects,[31] since carrier concentrations in all the samples were $\sim 10^{20}$ cm$^{-3}$ and lower, the Burstein–Moss model predicts a $N^{2/3}$ (carrier concentration obtained from Hall measurements) dependency of $\Delta E_G$ (the difference between the measured band gap of AZO films and the band gap of the pure ZnO thin film in this work). Such a plot of $N^{2/3}$ versus $\Delta E_G$ is shown in Fig. 8(b). A linear trend is only observed until at. % Al of 3.0%. Beyond this value of doping, the carrier concentration does not depend linearly on the substitutionally doped $Al^{3+}$ ions anymore, indicating a change in the mechanism and reduction in formation of free charge carriers. This trend seems consistent with the XRD, electrical and optical data.

The results in this paper demonstrate certain characteristics of ALD-based AZO films as compared to currently established methods of deposition. First, ALD can easily be used to dope ZnO and other oxide films by simply changing the sequence of precursor pulses. No target preparation (as in sputtering or PLD) or flow optimization (as in CVD) are required to get precise and highly uniform films. Second, ALD provides a unique tool to manipulate crystallographic orientation of AZO films. As shown in the past, this can be done by varying temperature pulse and purge times. In this paper, we show that a similar effect can be achieved with doping ZnO films as well. Third, given the low temperature of deposition and the ability of ALD to place monolayers of disparate materials contiguously to one another, many metastable phases could be accessed which may be harder to obtain using previously demonstrated deposition processes. Finally, given these characteristics of ALD-based AZO films, it is interesting to note that the film is optimized for resistivity at the same at. % Al as reported largely in literature.

## IV. CONCLUSION

AZO thin films of 100 nm thickness were prepared by systematically changing the number of DEZ-DI water cycles inserted between two TMA-DI water cycles at 150 °C by an ALD method. Whereas, pure ZnO film was polycrystalline, the AZO films crystallized preferentially along the [100] direction as a result of doping with Al. A single TMA-DI water cycle could remarkably reduce the roughness of ZnO films, highlighting its potential use for TCO based applications. The lowest resistivity of $4.5 \times 10^{-3}$ $\Omega$ cm was observed for AZO films $\sim$100 nm thick and grown with 3.0 at. % Al doping concentration (i.e., with 20 DEZ-DI water cycles for every single TMA-DI water cycle). Transmittances of over 80% were observed in the visible region for the films. The band gap of AZO increased with increasing Al doping concentration. However, the Burstein–Moss effect is only responsible for increase in the band gap until about 3.0 at. % Al.

It was found that at low at. % Al doping (3.0 at. % Al and lower), AZO films behave as substitutionally-doped TCO, where the properties of the ZnO are perturbed due to the presence of $Al^{3+}$ ions on $Zn^{2+}$ sites. This results in AZO films with a high degree of crystallinity, low resistivity and an increase in band gap consistent with the Burstein–Moss effect. At higher at. % Al (3.0 at. % and higher), structural, electrical, and optical properties indicate the formation of a possible metastable phase as predicted in a recent published work.[20] This effect is manifested in the AZO films as a decrease in crystallinity, an increase in resistivity and deviation from the Burstein–Moss effect.

## ACKNOWLEDGMENTS

This work was supported as part of the Science of Precision Multifunctional Nanostructures for Electrical Energy Storage, an Energy Frontier Research Center funded by the U.S. Department of Energy, Office of Science, Office of Basic Energy Sciences under Award No. DESC0001160. W.J.L. wishes to acknowledge the support by Dong-eui University Foundation Grant (2009). P.B. wishes to acknowledge the John and Maureen Hendricks Fellowship for support. The authors wish to thank the support of the Maryland NanoCenter including the NispLab and FabLab. S.B.L. was also supported by WCU program through the KOSEF funded by the MEST (Grant No. R31-2008-000-10071-0).

[1] *Zinc Oxide Bulk, Thin Films and Nanostructures*, edited by C. Jagadish and S. Pearton (Elsevier, Oxford, UK, 2006).
[2] J. N. Duenow, T. A. Gessert, D. M. Wood, T. M. Barnes, M. Young, B. To, and T. J. Coutts, J. Vac. Sci. Technol. A **25**, 955 (2007).
[3] T. Minami, H. Nanto, and S. Takata, Jpn. J. Appl. Phys., Part 2 **23**, L280 (1984).
[4] F. K. Shan, G. X. Liu, W. J. Lee, and B. C. Shin, J. Appl. Phys. **101**, 053106 (2007).
[5] *Transparent Conductive Zinc Oxide*, edited by K. Ellmer, A. Klein, and B. Rech (Springer, Berlin, Germany, 2008), Vol. 104.
[6] W. S. Lau and S. J. Fonash, J. Electron. Mater. **16**, 141 (1987).
[7] S. M. George, A. W. Ott, and J. W. Klaus, J. Phys. Chem. **100**, 13121 (1996).
[8] J. W. Elam and S. M. George, Chem. Mater. **15**, 1020 (2003).
[9] J. W. Elam, D. Routkevitch, and S. M. George, J. Electrochem. Soc. **150**, G339 (2003).
[10] J. W. Elam, Z. A. Sechrist, and S. M. George, Thin Solid Films **414**, 43 (2002).
[11] E. Guziewicz, I. A. Kowalik, M. Godlewski, K. Kopalko, V. Osinniy, A. Wojcik, S. Yatsunenko, E. Lusakowska, W. Paszkowicz, and M. Guziewicz, J. Appl. Phys. **103**, 033515 (2008).
[12] P. C. Rowlette, C. G. Allen, O. B. Bromley, A. E. Dubetz, and C. A. Wolden, Chem. Vapor Deposition **15**, 15 (2009).
[13] Q. H. Li, D. L. Zhu, W. J. Liu, Y. Liu, and X. C. Ma, Appl. Surf. Sci. **254**, 2922 (2008).
[14] See supplementary material at http://dx.doi.org/10.1063/1.3466987 for (EDX data showing Zn ti Si peak ratio used to normalize XRD data).
[15] J. Mass, P. Bhattacharya, and R. S. Katiyar, Mater. Sci. Eng., B **103**, 9 (2003).
[16] J. G. Lu, S. Fujita, T. Kawaharamura, H. Nishinaka, Y. Kamada, T. Ohshima, Z. Z. Ye, Y. J. Zeng, Y. Z. Zhang, L. P. Zhu, H. P. He, and B. H. Zhao, J. Appl. Phys. **101**, 083705 (2007).
[17] S. Y. Pung, K. L. Choy, X. Hou, and C. X. Shan, Nanotechnology **19**, 435609 (2008).
[18] E. B. Yousfi, J. Fouache, and D. Lincot, Appl. Surf. Sci. **153**, 223 (2000).
[19] D. Lide, *CRC Handbook of Chemistry and Physics*, 88th ed. (CRC, Boca Raton, FL, 2007).
[20] S. Yoshioka, F. Oba, R. Huang, I. Tanaka, T. Mizoguchi, and T. Yamamoto, J. Appl. Phys. **103**, 014309 (2008).
[21] M. H. Yoon, S. H. Lee, H. L. Park, H. K. Kim, and M. S. Jang, J. Mater. Sci. Lett. **21**, 1703 (2002).
[22] J. Hüpkes, B. Rech, S. Calnan, O. Kluth, U. Zastrow, H. Siekmann, and

Downloaded 17 Apr 2013 to 143.248.118.125. This article is copyrighted as indicated in the abstract. Reuse of AIP content is subject to the terms at: http://jap.aip.org/about/rights_and_permissions

M. Wuttig, Thin Solid Films **502**, 286 (2006).
[23]R. E. Hummel, *Electronic Properties of Materials*, 2nd ed. (Springer-Verlag, Berlin, Germany, 1993).
[24]J. G. Lu, Z. Z. Ye, Y. J. Zeng, L. P. Zhu, L. Wang, J. Yuan, B. H. Zhao, and Q. L. Liang, J. Appl. Phys. **100**, 073714 (2006).
[25]G. D. Wilk, R. M. Wallace, and J. M. Anthony, J. Appl. Phys. **89**, 5243 (2001).
[26]E. Burstein, Phys. Rev. **93**, 632 (1954).
[27]T. S. Moss, Proc. Phys. Soc. London, Sect. B **67**, 775 (1954).
[28]V. K. Miloslavskii and P. S. Pogrebniak, Phys. Status Solidi B **51**, K99 (1972).
[29]R. K. Shukla, A. Srivastava, and K. C. Dubey, J. Cryst. Growth **294**, 427 (2006).
[30]J. H. Wang, L. Meng, Y. Qi, M. L. Li, G. M. Shi, and M. L. Liu, J. Cryst. Growth **311**, 2305 (2009).
[31]K. F. Berggren and B. E. Sernelius, Phys. Rev. B **24**, 1971 (1981).

Downloaded 17 Apr 2013 to 143.248.118.125. This article is copyrighted as indicated in the abstract. Reuse of AIP content is subject to the terms at: http://jap.aip.org/about/rights_and_permissions